Journal of Turbulence
Volume 7, No. 38, 2006

Taylor & Francis
Taylor & Francis Group

Application of Taylor series expansion and Least-squares-based lattice Boltzmann method to simulate turbulent flows

C. SHU*, Y. PENG, C. F. ZHOU, and Y. T. CHEW

Department of Mechanical Engineering, National University of Singapore, 10 Kent Ridge Crescent, 117576 Singapore

Lattice Boltzmann method (LBM) has become an alternative method of computing a variety of fluid flows, ranging from low Reynolds number laminar flows to highly turbulent flows. For turbulent flows, non-uniform grids are preferred. Taylor series expansion- and least-squares-based LBM (TLLBM) is an effective and convenient way to extend standard LBM to be used on arbitrary meshes. In order to show its ability to solve turbulent flows, we combine it with k–ω and S-A turbulence models. To validate these combinations, the benchmark problems of the turbulent channel flow and the turbulent flow over a backward facing step at $Re = 44\,000$ are simulated. Our results compare well with the analytical solution and the experimental results of Kim *et al.* [22]. This shows that the combination of TLLBM with turbulence model can solve turbulent flows effectively.

1. Introduction

In recent decades, lattice Boltzmann method has received considerable attention as an alternative method of computing a variety of fluid flows, ranging from low Reynolds number laminar flows to highly turbulent flows [1–7]. For turbulent flows, large computation times can be reduced by using nonuniform grids with the resolution concentrated in the regions where the turbulence is most intense. Several researchers have extended the standard LBM to nonuniform lattices. Nannelli and Succi [8], Amati *et al.* [9] and Chen [10] developed a finite-volume version of LBM (FVLBM) that involves a non-uniform coarse lattice containing several basic lattice cells. A new FVLBM is proposed by Peng *et al.* [11], which can be used on irregular meshes with arbitrary connectivity. It is based on modern finite-volume methods and keeps the simplicity of the conventional LBM. Filippova and Hanel [12] proposed a local grid refinement method based on the hierarchical grid refinement in conventional CFD methods. McNamara *et al.* [13] presented the Lax-Wendroff LBM scheme. He and Doolen [14] proposed a method called the interpolation-supplemented lattice Boltzmann equation model (ISLBE). This method applies the interpolation to update the particle distribution functions on the coarse portion of the grid after the propagation step. Quadratic upwind interpolation was used to obtain the result with second order of accuracy. Lee and Lin [15, 16] presented a new strategy in which the streaming step is carried out by solving pure linear advection equations in an Eulerian framework. Recently, a new version of LBM called Taylor series expansion- and least squares-based LBM (TLLBM), derived from the standard LBM by using Taylor

*Corresponding author. E-mail: mpeshuc@nus.edu.sg.

Journal of Turbulence
ISSN: 1468-5248 (online only)
http://www.tandf.co.uk/journals
DOI: 10.1080/14685240600677624

series expansion and optimized by the least squares method, is presented by Shu *et al.* [17]. It has the following good properties: it has an explicit algebraic form; there is no requirement for the selection of neighboring points, so it is nothing to do with the mesh structure; it can be uniformly applied to different lattice models. Compared with ISLBE, the selection of the upwind points required by ISLBE for the stability reason is not necessary for TLLBM. It can randomly select neighboring points. It has been successfully used to solve many practical laminar flows on arbitrary meshes. This motivates our present study. In this work, we try to extend TLLBM to simulate turbulent flows with use of highly clustered meshes near wall boundaries.

For turbulent flows, a wide range of eddy scales exist. Theoretically, the lattice Boltzmann method should be able to resolve all these scales and provide detailed features of flow turbulence. However, such a direct simulation except for simple flows will be far beyond the present and foreseeable computing power. Consequently, turbulence modeling is preferred. It can be classified into algebraic model, one-equation model, two-equation model, Reynolds stress model and other complex models. The simplest one is the algebraic model. However, it needs a lot of special empiricism. For a one-equation model, such as S-A turbulent model [18], there is only one evolution equation governing the evolution of eddy viscosity. It is easy to implement. Furthermore, it tends to be LES SGS model when the refined length scale is introduced. This is a quite new approach for the treatment of turbulence called DES [19]. Among the turbulence models used today, two-equation eddy-viscosity models appear to be favored because they incorporate substantially more turbulence physics and less special empiricism than algebraic models while avoiding difficulties in numerical implementation and excessive computational cost as compared with other more complex models. Among two-equation eddy-viscosity models, the k–ε model by Launder and Spalding [20] is probably the most popular. To do the integration to the wall, the standard form of the k–ε model needs to be modified by introducing damping functions to take the low Reynolds number effects into account. However, the k–ε model fails to predict flows with strong adverse pressure gradients accurately although it is a good choice for large number of flow fields [21]. Compared with the k–ε model, the k–ω model is easier to be integrated through the viscous sub-layer since it does not require additional damping functions at low Reynolds number. More importantly, it was designed to achieve more accurate predictions for adverse pressure gradient flows [21]. The problem of k–ω model is its difficulty to deal with higher y^+ near the wall. The Reynolds stress model is more complicated and it incorporates more physics into the model. To couple the turbulence modeling with LBM, the single relaxation time is modified as a variable relaxation time which is directly linked to the turbulent viscosity [3]. Some research work has been done in which the turbulent viscosity is determined by the solution of two differential equations [4, 5], or a subgrid-scale (SGS) stress model [6, 7]. In this paper, we combined TLLBM with the turbulence modeling and the turbulent viscosity was calculated by S-A model and k–ω model, respectively.

In order to validate the combination of TLLBM with the turbulence model, the turbulent channel flow is calculated using k–ω model. Then the benchmark problem of the turbulent flow over a backward facing step at $Re = 44\,000$ is simulated in detail using S-A model and k–ω model. Our results compare well with the experimental results of Kim *et al.* [22]. This shows that the combination of TLLBM with turbulence model can solve turbulent flows effectively.

2. Taylor series expansion and least-squares-based LBM (TLLBM)

2.1 *The scheme of TLLBM*

The TLLBM is based on the well-known fact that the distribution function is a continuous function in physical space and can be well defined in any mesh system. The details of TLLBM can be found in [17]. Some basic description of TLLBM is shown below.

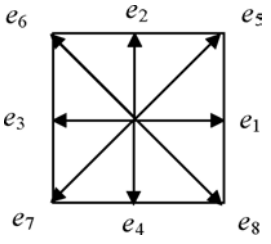

Figure 1. Configuration of the 9-bit model.

The two-dimensional, standard LBE with BGK approximation can be written as

$$f_i(x + e_{ix}\delta t, y + e_{iy}\delta t, t + \delta t) = f_i(x, y, t) + \frac{f_i^{\mathrm{eq}}(x, y, t) - f_i(x, y, t)}{\tau} \qquad i = 0, 1, \ldots, N, \tag{1}$$

where τ is the single relaxation time; f_i is the distribution function along the i direction; f_i^{eq} is its corresponding equilibrium state; δt is the time step and $e_i(e_{ix}, e_{iy})$ is the particle velocity in the i direction; N is the number of discrete particle velocities. In this paper, the nine-bit model is used. The schematic description of this model is shown in figure 1.

Suppose that a particle is initially at the grid point (x, y, t). Along the i direction, this particle will stream to the position $(x + e_{ix}\delta t, y + e_{iy}\delta t, t + \delta t)$. For a uniform lattice, $\delta x = e_{ix}\delta t$, $\delta y = e_{iy}\delta t$. So, $(x + e_{ix}\delta t, y + e_{iy}\delta t)$ is at the grid point. In other words, equation (1) can be used to update the distribution functions exactly at the grid points. However, for a non-uniform grid, $(x + e_{ix}\delta t, y + e_{iy}\delta t)$ is usually not at the grid point $(x + \delta x, y + \delta y)$. In the numerical simulation, only the distribution functions at the mesh points for all the time levels are needed, so that the macroscopic properties such as the density, flow velocity and temperature can be evaluated at every mesh point. To get the distribution function at the grid point $(x + \delta x, y + \delta y)$ and the time level $t + \delta t$, the Taylor series expansion in the spatial direction is applied.

As shown in figure 2, for simplicity, the point A represents the grid point (x_A, y_A, t), point A' represents the position $(x_A + e_{ix}\delta t, y_A + e_{iy}\delta t, t + \delta t)$, and point P represents the position $(x_P, y_P, t + \delta t)$ with $x_P = x_A + \delta x$, $y_P = y_A + \delta y$. So, equation (1) gives

$$f_i(A', t + \delta t) = f_i(A, t) + \left[f_i^{\mathrm{eq}}(A, t) - f_i(A, t)\right]/\tau. \tag{2}$$

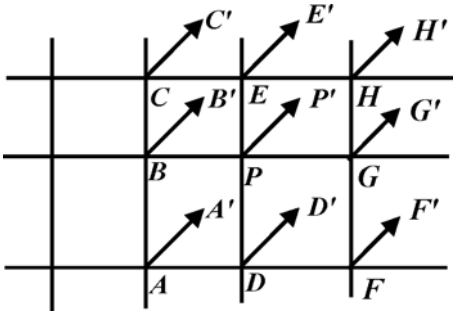

Figure 2. Configuration of particle movement along the i direction.

For the general case, A' may not coincide with the mesh point P. We truncate the Taylor series expansion to the second-order derivative terms. So $f_i(A', t+\delta t)$ can be approximated by the corresponding function and its derivatives at the mesh point Pas

$$f_i(A', t+\delta t) = f_i(P, t+\delta t) + \Delta x_A \frac{\partial f_i(P, t+\delta t)}{\partial x} + \Delta y_A \frac{\partial f_i(P, t+\delta t)}{\partial y} + \frac{1}{2}(\Delta x_A)^2 \frac{\partial^2 f_i(P, t+\delta t)}{\partial x^2} + \frac{1}{2}(\Delta y_A)^2 \frac{\partial^2 f_i(P, t+\delta t)}{\partial y^2} + \Delta x_A \Delta y_A \frac{\partial^2 f_i(P, t+\delta t)}{\partial x \partial y} + O[(\Delta x_A)^3, (\Delta y_A)^3], \tag{3}$$

where $\Delta x_A = x_A + e_{ix}\delta t - x_P$ and $\Delta y_A = y_A + e_{iy}\delta t - y_P$. For the two-dimensional case, this expansion involves six unknowns, that is, one distribution function at the time level $t+\delta t$, two first-order derivatives and three second-order derivatives. To solve for these unknowns, six equations are needed to close the system. This can be done by applying the second-order Taylor series expansion to six points: P, A, B, C, D, E. As shown in [17], the following equation system can be obtained:

$$f'_k = \{s_k\}^T \{W\} = \sum_{j=1}^{6} s_{k,j} W_j \quad k = P, A, B, C, D, E, \tag{4}$$

where

$$f'_k = f_i(x_k, y_k, t) + \left[f_i^{\mathrm{eq}}(x_k, y_k, t) - f_i(x_k, y_k, t)\right]/\tau$$
$$\{s_k\}^T = \{1, \Delta x_k, \Delta y_k, (\Delta x_k)^2/2, (\Delta y_k)^2/2, \Delta x_k \Delta y_k\}$$
$$\{W\} = \{f_i, \partial f_i/\partial x, \partial f_i/\partial y, \partial^2 f_i/\partial x^2, \partial^2 f_i/\partial^2 y, \partial^2 f_i/\partial x \partial y\}^T.$$

Our target is to find the first element $W_1 = f_i(P, t+\delta t)$. Equation (4) can be put into the following matrix form:

$$[S]\{W\} = \{f'\}. \tag{5}$$

In practical applications, it was found that the matrix $[S]$ might be singular or ill conditioned using only six points (P, A, B, C, D and E). To overcome this difficulty and make the method more general, more points are added and the least-squares approach [23] was introduced to optimize the over-constrained approximation by equation (5). As a result, the equation system for W becomes

$$\{W\} = ([S]^T[S])^{-1}[S]^T\{f'\} = [A]\{f'\}. \tag{6}$$

From equation (6), we can have

$$f_i(x_0, y_0, t+\delta t) = W_1 = \sum_{k=1}^{M} a_{1,k} f'_k, \tag{7}$$

where $a_{1,k}$ are the elements of the first row of the matrix $[A]$, which is determined by the coordinates of mesh points, the particle velocity and time-step size, and will not be changed in the calculation procedure. M is the number of the points used and should be greater than 6. In the present study, a structured grid is used, and M is taken as 9. This means that for a reference mesh point P, we need to select its eight neighboring points to compute the coefficients in equation (7). Figure 2 shows the actual point distribution used in the present study. Although

it is illustrated along the particle direction of 45°, the point distribution shown in figure 2 can be applied to other particle directions including the horizontal and vertical directions. We can calculate the coefficients in equation (7) once and store them in advance, so little computational effort is introduced as compared with the standard LBE. On the other hand, equation (7) has nothing to do with the mesh structure. It only needs the information of coordinates of the mesh points. Thus, we can say that equation (7) can be consistently used to any kind of mesh structure. But we have to indicate that, as compared to the standard LBE, the present method requires much more memory to store the coefficients $a_{1,k}$.

Once the density distribution function is obtained, the macroscopic density ρ and momentum density $\rho\mathbf{U}$ are computed by

$$\rho = \sum_{\alpha=0}^{M} f_\alpha, \quad \rho\mathbf{U} = \sum_{\alpha=0}^{M} f_\alpha \mathbf{e}_\alpha.$$

2.2 *Boundary condition*

At the boundary, the values of outgoing distributions are determined from equation (7) and the incoming distributions are determined from boundary conditions. In this paper, there are inflow, outflow, solid wall and symmetry plane boundary conditions.

For the wall boundary, the bounce-back scheme is used. Take the bottom wall as an example. f_2, f_5 and f_6 are incoming distributions. Their values are determined respectively from $f_2 = f_4$, $f_5 = f_7$ and $f_6 = f_8$.

For the inflow boundary with given velocity, the non-equilibrium extrapolation method [24] is used. At this boundary, f_1, f_5 and f_8 are incoming distributions. Their values are determined respectively from $f_1^{\mathrm{neq}} = f_3^{\mathrm{neq}}$, $f_5^{\mathrm{neq}} = f_7^{\mathrm{neq}}$ and $f_8^{\mathrm{neq}} = f_6^{\mathrm{neq}}$. The given velocity is used when calculating the equilibrium distributions.

For the outlet boundary condition, the extrapolation scheme is used.

For the symmetry plane, one ghost grid line is used. The values on the ghost grid are determined from the symmetry condition. For example, if the symmetry plane is indexed by *jm*, the line below this plane is indexed by $jm - 1$ and the ghost grid line which is symmetric to the line $jm - 1$ with respect to *jm* is indexed by *jmax*, the values on the ghost grid are determined by

$$\begin{aligned}
&f_1^{j\,\max} = f_1^{jm-1}, \quad f_2^{j\,\max} = f_4^{jm-1}, \quad f_3^{j\,\max} = f_3^{jm-1},\\
&f_4^{j\,\max} = f_2^{jm-1}, \quad f_5^{j\,\max} = f_8^{jm-1}, \quad f_6^{j\,\max} = f_7^{jm-1},\\
&f_7^{j\,\max} = f_6^{jm-1}, \quad f_8^{j\,\max} = f_5^{jm-1}, \quad f_9^{j\,\max} = f_9^{jm-1}.
\end{aligned}$$

3. Turbulence modeling

For turbulent flows, the relaxation time τ in equation (1) is determined from the effective viscosity. The effective viscosity, which is the summation of the turbulent viscosity and molecular viscosity, is related to the relaxation time by

$$\upsilon = \upsilon_{\mathrm{l}} + \upsilon_{\mathrm{t}} = \left(\tau - \frac{1}{2}\right) c_{\mathrm{s}}^2 \delta t, \tag{8}$$

where υ_{l} means the molecular viscosity and υ_{t} means the turbulent viscosity. υ_{t} is determined from the turbulence modeling.

3.1 *k–ω turbulence modeling*

The turbulent viscosity in equation (8) is determined from the Wilcox k–ω turbulence model, which is

$$\nu_{\mathrm{t}} = \frac{k}{\omega} \tag{9}$$

$$\frac{\partial k}{\partial t} + \frac{\partial (uk)}{\partial x} + \frac{\partial (vk)}{\partial y} = \nu_{\mathrm{t}} P_{\mathrm{d}} + \frac{\partial}{\partial x}\left[(\nu_{\mathrm{l}} + \sigma_k \nu_{\mathrm{t}})\frac{\partial k}{\partial x}\right] + \frac{\partial}{\partial y}\left[(\nu_{\mathrm{l}} + \sigma_k \nu_{\mathrm{t}})\frac{\partial k}{\partial y}\right] - \beta_k k\omega \tag{10}$$

$$\frac{\partial \omega}{\partial t} + \frac{\partial (u\omega)}{\partial x} + \frac{\partial (v\omega)}{\partial y} = \gamma_\omega P_{\mathrm{d}} + \frac{\partial}{\partial x}\left[(\nu_{\mathrm{l}} + \sigma_\omega \nu_{\mathrm{t}})\frac{\partial \omega}{\partial x}\right] + \frac{\partial}{\partial y}\left[(\nu_{\mathrm{l}} + \sigma_\omega \nu_{\mathrm{t}})\frac{\partial \omega}{\partial y}\right] - \beta_\omega \omega^2 \tag{11}$$

where $P_{\mathrm{d}} = 2[(\frac{\partial u}{\partial x})^2 + (\frac{\partial v}{\partial y})^2] + (\frac{\partial u}{\partial y} + \frac{\partial v}{\partial x})^2$.

The closure coefficients for the Wilcox k–ω model are

$$\beta_k = 0.09 \quad \sigma_k = 0.5 \quad \beta_\omega = 0.075 \quad \sigma_\omega = 0.5 \quad \gamma_\omega = 5/9.$$

To solve equations (11) and (11), they are rewritten into the advection-diffusion form [25, 26]

$$\frac{\partial A}{\partial t} + \tilde{u}_j \frac{\partial A}{\partial x_j} = D_A \frac{\partial^2 A}{\partial x_j^2} + S_A \tag{12}$$

where A denotes either of the turbulent quantities k or ω; D_A is $\nu_{\mathrm{l}} + \sigma_k \nu_{\mathrm{t}}$ for k equation and it is $\nu_{\mathrm{l}} + \sigma_\omega \nu_{\mathrm{t}}$ for ω equation; S_A is the source term, which is $\nu_{\mathrm{t}} P_{\mathrm{d}} - \beta_k k\omega$ for k equation and is $\gamma_\omega P_{\mathrm{d}} - \beta_\omega \omega^2$ for ω equation; $\tilde{u}_j$ is the effective velocity, which is $u_j - \frac{\partial D_A}{\partial x_j}$. Equation (12) is solved by a Lax–Wendroff-like finite difference discretization on the non-uniform mesh. Assume A_{l} is the value of local point under consideration; A_{b} is the value of backward point located at a distance d_{b} away from the local point; A_{f} is the value of forward point located at distance d_{f} away. The mesh non-uniformity Ω is defined as $\Omega = \frac{d_{\mathrm{f}} - d_{\mathrm{b}}}{d_{\mathrm{f}} + d_{\mathrm{b}}} = \frac{d_{\mathrm{f}} - d_{\mathrm{b}}}{2\Delta x_j}$ along the x_j-direction. Then the discretization form of equation (12) is written as

$$A^{n+1} = A_m - \frac{\Delta t}{\Delta x_j}\tilde{u}_j F_j + \left(\frac{\Delta t^2}{2(\Delta x_j)^2}\tilde{u}_j^2 + \frac{\Delta t}{(\Delta x_j)^2} D_A\right) G_j - \frac{1}{2D}\sum_j G_j + \Delta t S_A, \tag{13}$$

where

$$A_m = \sum_j \frac{1}{D} A_{jm}, \text{ in which } A_{jm} = \frac{1}{2}\left(A_{\mathrm{f}} + A_{\mathrm{l}} + (A_{\mathrm{b}} - A_{\mathrm{l}})\frac{d_{\mathrm{f}}}{d_{\mathrm{b}}}\right),$$

$$F_j = \frac{\Delta x_j}{2}\left(\frac{(1-\Omega)(A_{\mathrm{f}} - A_{\mathrm{l}})}{d_{\mathrm{f}}} - \frac{(1+\Omega)(A_{\mathrm{b}} - A_{\mathrm{l}})}{d_{\mathrm{b}}}\right),$$

$$G_j = \Delta x_j \left(\frac{(A_{\mathrm{f}} - A_{\mathrm{l}})}{d_{\mathrm{f}}} + \frac{(A_{\mathrm{b}} - A_{\mathrm{l}})}{d_{\mathrm{b}}}\right).$$

The boundary conditions encountered in this paper when solving k–ω equations are classified into inflow, outflow, solid wall and symmetry plane boundary conditions. At the inflow boundary, the non-dimensional form of k and ω are set at very low levels, i.e.

$$k_{\mathrm{in}} = 1.5 I_{\mathrm{T}}^2 u_{\mathrm{in}}^2 \qquad \omega_{\mathrm{in}} = \frac{\sqrt{k_{\mathrm{in}}}}{C_\mu^{1/4} l_{\mathrm{in}}}, \tag{14}$$

where I_T is the turbulence intensity, usually taken to be 3%, $C_\mu = 0.09$ and l_{in} is the length scale given by

$$l_{in} = \min(\kappa y_{wall}, 0.1H). \tag{15}$$

Here y_{wall} is the normal distance from the wall and $\kappa = 0.41$ denotes the universal von Karman constant.

At the outflow boundary, the streamwise gradients of k and ω are assumed to be zero, i.e.

$$\frac{\partial k}{\partial x} = \frac{\partial \omega}{\partial x} = 0. \tag{16}$$

The non-slip wall boundary conditions for k–ω model equations are

$$k = 0 \rightarrow \omega = \frac{6\nu_l}{\beta_\omega y_1^2}. \tag{17}$$

For the symmetry plane boundary, the gradients of k and ω in y-direction are assumed to be zero, i.e.

$$\frac{\partial k}{\partial y} = \frac{\partial \omega}{\partial y} = 0. \tag{18}$$

3.2 *S-A turbulence modeling*

The completed S-A model is described as follows. The turbulent viscosity ν_t is given by

$$\nu_t = \tilde{\nu} f_{\upsilon 1}, \quad f_{\upsilon 1} = \frac{\chi^3}{\chi^3 + c_{\upsilon 1}^3}, \quad \chi \equiv \frac{\tilde{\nu}}{\nu_l}. \tag{19}$$

$\tilde{\nu}$ in equation (19) is the working variable and obeys the transport equation

$$\begin{aligned}\frac{D\tilde{\nu}}{Dt} &= c_{b1}[1 - f_{t2}]\tilde{S}\tilde{\nu} + \frac{1}{\sigma}[\nabla \cdot ((\nu_l + \tilde{\nu})\nabla\tilde{\nu}) + c_{b2}(\nabla\tilde{\nu})^2] \\ &\quad - \left[c_{w1} f_w - \frac{c_{b1}}{k^2} f_{t2}\right]\left[\frac{\tilde{\nu}}{d}\right]^2 + f_{t1}\Delta U^2,\end{aligned} \tag{20}$$

where

$$\tilde{S} \equiv S + \frac{\tilde{\nu}}{k^2 d^2} f_{\upsilon 2}, \quad f_{\upsilon 2} = 1 - \frac{\chi}{1 + \chi f_{\upsilon 1}}, \tag{21}$$

in which S is the magnitude of vorticity and d is the distance to the closet wall.

Two functions f_w and f_{t2} in equation (20) are defined as

$$f_w = g\left[\frac{1 + c_{w3}^6}{g^6 + c_{w3}^6}\right]^{1/6}, \quad g = r + c_{w2}(r^6 - r), \quad r \equiv \frac{\tilde{\nu}}{\tilde{S}k^2 d^2}. \tag{22}$$

$$f_{t2} = c_{t3} \exp(-c_{t4}\chi^2). \tag{23}$$

The trip function f_{t1} in equation (20) is as follows:

$$f_{t1} = c_{t1} g_t \exp\left(-c_{t2}\frac{\omega_t^2}{\Delta U^2}\left[d^2 + g_t^2 d_t^2\right]\right), \tag{24}$$

where d_t is the distance from the field point to the trip, which is on the wall; ω_t is the wall vorticity at the trip; ΔU is the difference between the velocity at the field point and that at the trip; $g_t \equiv \min(0.1, \Delta U/\omega_t \Delta x)$ where Δx is the grid spacing along the wall at the trip.

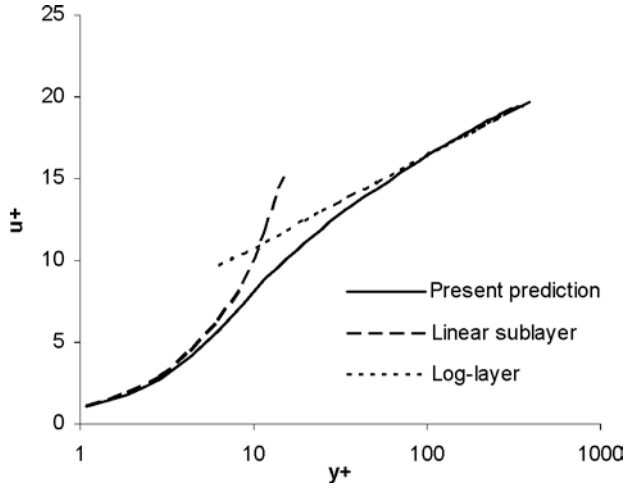

Figure 3. Velocity distribution in the viscous sub-layer and logarithmic layer.

The constants in S-A model are taken as $c_{b1} = 0.1355$, $\sigma = 2/3$, $c_{b2} = 0.622$, $k = 0.41$, $c_{w1} = c_{b1}/k^2 + 1 + c_{b2})/\sigma, c_{w2} = 0.3, c_{w3} = 2, c_{\upsilon 1} = 7.1, c_{t1} = 1, c_{t2} = 2, c_{t3} = 1.1, c_{t4} = 2$.

To solve equation (20), Euler integration algorithm is used for the time integration. The second-order upwind-biased scheme is used to deal with the convective terms.

The boundary conditions encountered in this paper when solving S-A equations are classified as inflow, outflow and solid wall boundary conditions. At the inflow, $\tilde{\nu}$ is set at very low levels, usually several times that of molecular viscosity. At the outflow boundary, the streamwise gradients of $\tilde{\nu}$ is assumed to be zero, i.e. $\frac{\partial \tilde{\nu}}{\partial x} = 0$. For the no-slip wall boundary condition, $\tilde{\nu}$ is zero.

4. Numerical results and discussion

To see whether the law of wall can be properly recovered, the turbulent channel flow using TLLBM with k–ω model at $Re_H = 13\,750$ is studied. The Reynolds number Re_H is based on the channel height and the average inlet velocity. The computation is performed on a nonuniform grid of 261 × 81. The first line closest to the wall surface lies below $y^+ = 1$ from the wall. The calculated profile of velocity distribution is displayed in figure 3.

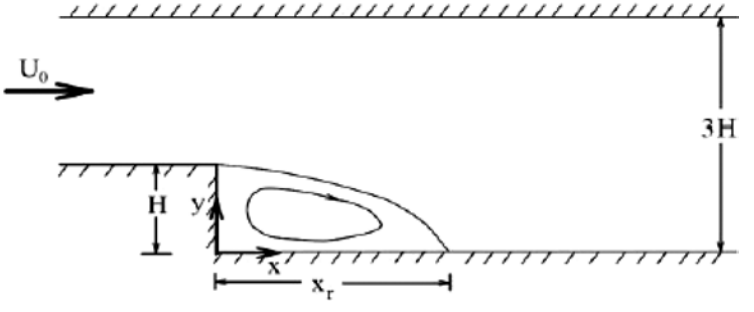

Figure 4. Domain configuration for the backward facing step.

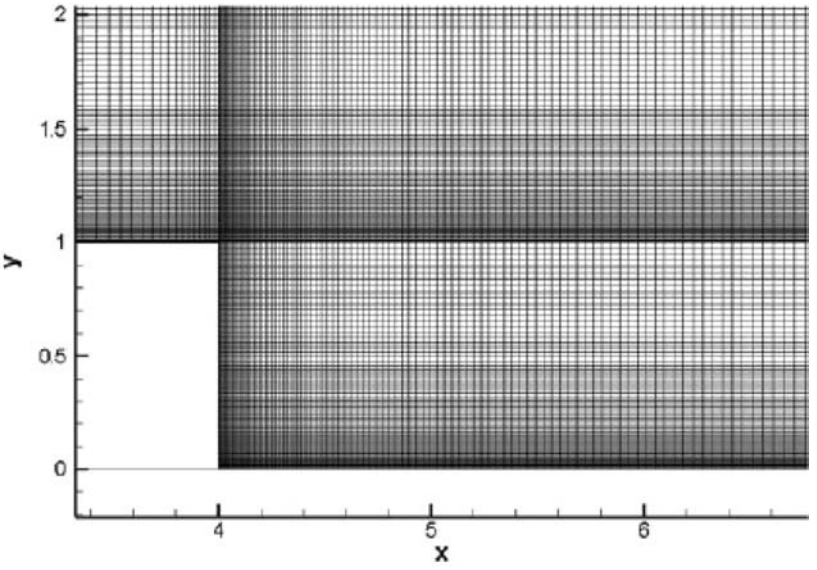

Figure 5. Typical mesh for simulation.

In figure 3, an excellent agreement is observed between current velocity profile with the wall functions which include the theoretical linear sub-layer law $u^+ = y^+$ $(0 \leq y^+ \leq 5)$ and theoretical logarithmic law of the wall, given by

$$u^+ = \frac{1}{\kappa} \log y^+ + 5.1 \quad (30 \leq y^+ \quad \text{and} \quad y < 0.1\delta), \tag{25}$$

where $y^+ = \frac{yu_\tau}{\nu}$, $u^+ = \frac{u}{u_\tau}$.

Then the benchmark problem of the turbulent flow over a backward facing step at $Re = 44\,000$ using TLLBM with k–ω model and S-A model is simulated. Turbulent flow over a backward facing step is a widely used benchmark problem to evaluate the performance of turbulent models in the prediction of separated flows. It is well known that the standard k–ε with wall function under-predicts the reattachment length in the backward facing step by an amount of 20–25%. This has been widely discussed since the 1980–1981 AFOSR-HTTM Stanford conference on complex turbulent flows [27–29]. In this study, the flow configuration of Kim *et al.* [22] is chosen for the computation. The ratio of the step height to the outlet height

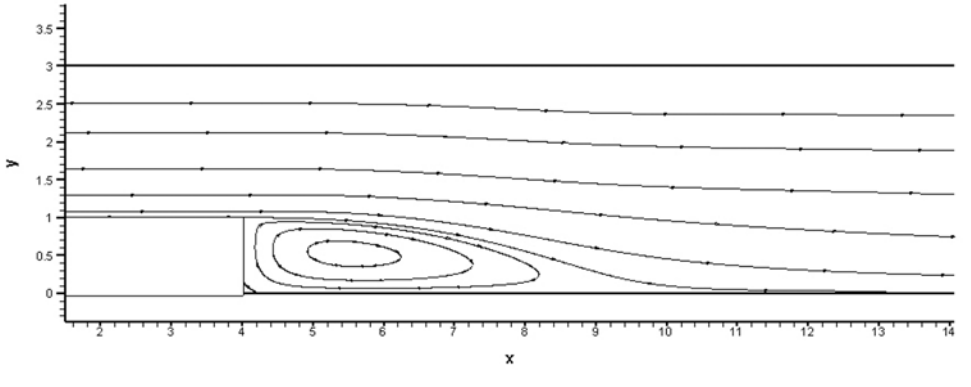

Figure 6. Streamlines for flow over a backward facing step at $Re = 44\,000$.

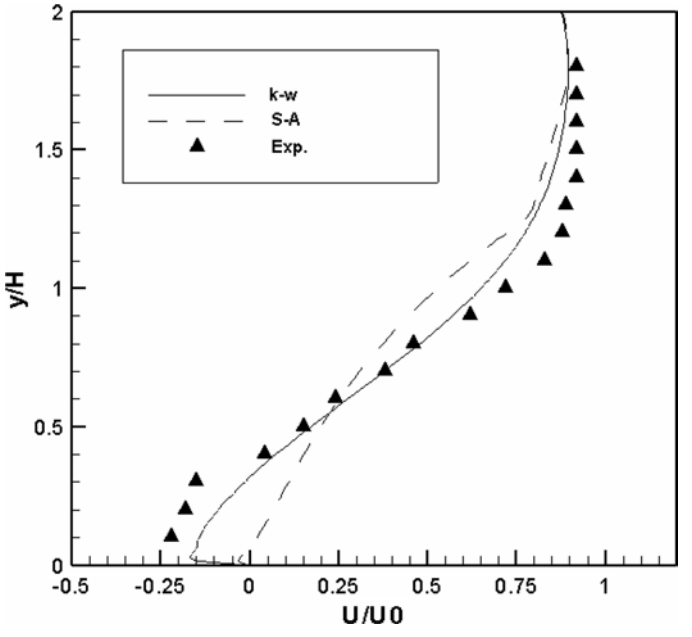

Figure 7. Velocity profile for flow over a backward facing step at $X = 5.33H$.

is 1:3 and the Reynolds number is based on the length scale of step height and the centerline velocity at the channel inlet. The domain configuration is shown in figure 4. The channel inlet is specified at four step heights upstream of the step corner. One-seventh law of the fully developed turbulent flow is used there for the given inlet velocity profile. The outlet is set at 20 step heights downstream of the step. Zero normal velocity gradient boundary condition is used there.

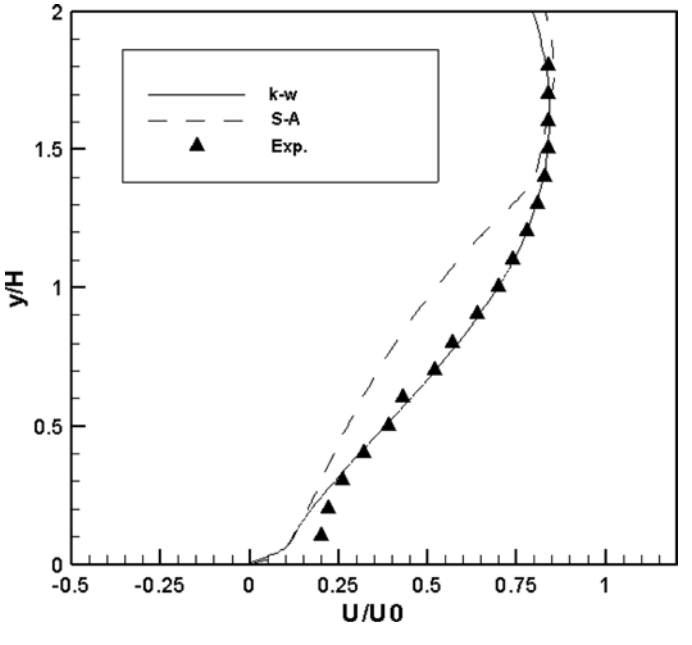

Figure 8. Velocity profile for flow over a backward facing step at $X = 8.00H$.

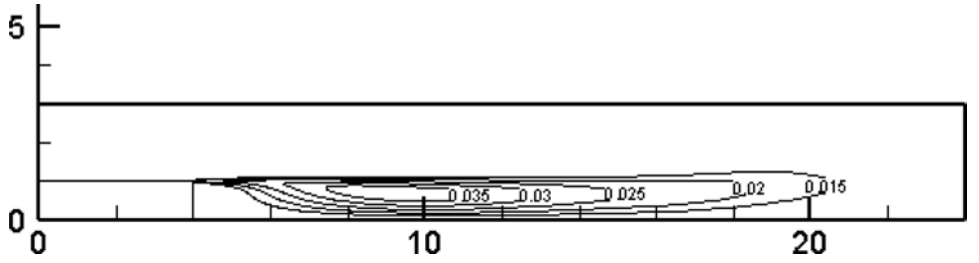

Figure 9. Turbulent intensity contours for flow over a backward facing step.

As shown in figure 5, the non-uniform orthogonal Cartesian mesh is applied in the computational domain. Grids are highly clustered around the step corner and near the wall regions.

The calculated reattachment length, named X_r in figure 4 is widely used as the criteria for the turbulence models. For $Re = 44\,000$, the reattachment length using S-A model is $X_r = 6.37H$, which agrees well with the prediction from the experiment of Kim *et al.* [22] that gave the reattachment length in the range of $X_r = (7.0 \pm 1.0)H$. The result from this work is much better than the prediction from the standard k–ε model with wall functions which under-predict the reattachment length. The obtained reattachment length for k–ω is $X_r = 7.00H$, which agrees better than S-A model compared with the experimental data. The typical streamlines of present simulation are shown in figure 6.

Streamwise velocity profiles are compared with the experimental data at the locations of $5.33H$ and $8.00H$. One location is before the reattachment point and the other is after the reattachment point. Velocity profiles at these two positions are shown in figures 7 and 8. From these two figures, we can see that the computed velocity profiles basically agree well with the experimental results. In figure 7, the velocity profile lies in the large separation region and RANS cannot get very accurate results in this region when compared with the experiment results. So there is some difference near the wall region. Between these two turbulence models, k–ω agrees better with the experimental results than S-A model. This phenomenon can be expected from the results of the reattachment length, since S-A model under-predicts the reattachment length about 9% as compared with the experiment results.

The typical turbulent intensity contours are shown in figure 9. From this figure, it can be seen that the strong turbulent intensity area lies in the high vorticity region which locates after the step corner. They agree well with the experimental results.

5. Conclusions

Taylor series expansion- and least-squares-based LBM (TLLBM) is an effective and convenient way to extend the standard LBM to be used on arbitrary meshes. It has the following good properties: It has an explicit algebraic form; there is no requirement for the selection of neighboring points, so it is nothing to do with the mesh structure; it can be uniformly applied to different lattice models. It has been successfully used to solve many practical laminar flows on arbitrary meshes. In this paper, we extended TLLBM to the simulations of turbulent flows. This can improve the efficiency for the simulation of turbulent flows since highly clustered meshes can be used near solid boundaries. The combination of TLLBM with k–ω model and S-A model is validated by applying it to simulate the benchmark problems of the turbulent channel flow and the turbulent flow over a backward facing step at $Re = 44\,000$. The obtained results compare well with the theoretical solution and experimental data of Kim *et al.* [22].

This shows that the combination of TLLBM with turbulence modeling can solve turbulent flows effectively.

References

[1] Chen, S. and Doolen, G.D., 1998, Lattice Boltzmann method for fluid flows. *Annual Review of Fluid Mechanics*, **30**, 329.

[2] Amati, G., Succi, S. and Benzi, R., 1997, Turbulent channel flow simulation using a coarse-grained extension of the lattice Boltzmann method. *Fluid Dynamics Research*, **19**, 289.

[3] Chen, H., Kandasamy, S., Orszag, S., Shock, R., Succi, S. and Yakhot, V., 2003, Extended Boltzmann kinetic equation for turbulent flows. *Science*, **301**, 633.

[4] Teixeira, C., 1998, Incorporating turbulence models into the lattice-Boltzmann method. *International Journal of Modern Physics C*, **9**(8), 1159.

[5] Filippova, O., Succi, S., Mazzocco, F., Arrighetti, C., Bella, G. and Hanel, D., 2001, Multiscale lattice Boltzmann schemes with turbulence modeling. *Journal of Computational Physics*, **170**, 812.

[6] Hou, S., Sterling, J., Chen, S. and Doolen, G.D., 1996, A lattice Boltzmann subgrid model for high Reynolds number flows. *Fields Institute Communications*, **6**, 151.

[7] Lu, Z., Liao, Y., Qian, D., McLaughlin, J.B., Derksen, J.J. and Kontomaris, K., 2002, Large eddy simulations of a stirred tank using the lattice Boltzmann method on a nonuniform grid. *Journal of Computational Physics*, **181**, 675.

[8] Nannelli, F. and Succi, S., 1992, The lattice Boltzmann equation on irregular lattices. *Journal of Statistical Physics*, **68**, 401.

[9] Amati, G., Succi, S. and Benzi, R., 1997, Turbulent channel flow simulation using a coarse-grained extension of the lattice Boltzmann method. *Fluid Dynamics Research*, **19**, 289.

[10] Chen, H., Volumetric formulation of the lattice Boltzmann method for fluid dynamics: basic concept. *Physical Review E*, **58**, 3955.

[11] Peng, G., Xi, H. and Duncan, C., 1998, Lattice Boltzmann method on irregular meshes. *Physical Review E*, **58**, 4124.

[12] Filippova, O. and Hanel, D., 1998, Grid refinement for lattice-BGK models. *Journal of Computational Physics*, **147**, 219.

[13] McNamara, G.R., Garcia, A.L. and Alder, B.J., 1995, Stabilization of thermal lattice Boltzmann models. *Journal of Statistical Physics*, **81**, 395.

[14] He, X. and Doolen, G.D., 1997, Lattice Boltzmann method on curvilinear coordinates system: flow around a circular cylinder. *Journal of Computational Physics*, **134**, 306.

[15] Lee, T. and Lin, C.L., 2003, An Eulerian description of the streaming process in the lattice Boltzmann equation. *Journal of Computational Physics*, **185**, 445.

[16] Lee, T. and Lin, C.L., 2001, A characteristic Galekin method for discrete Boltzmann equation. *Journal of Computational Physics*, **171**, 336.

[17] Shu, C., Chew, Y.T. and Niu, X.D., 2001, Least-squares-based lattice Boltzmann method: a meshless approach for simulation of flows with complex geometry. *Physical Review E*, **64**, 045701(R).

[18] Spalart, P.R. and Allmaras, S.R., 1994, A one-equation turbulence model for aerodynamic flows. *La Recherche A'erospatiale*, **1**, 5.

[19] Strelets, M., 2001, Detached eddy simulation of massively separated flows. AIAA paper, 2001-0879.

[20] Launder, B.E. and Spalding, D.B., 1974, The numerical computation of turbulent flows. *Computational Methods in Applied Mechanical Engineering*, **3**, 269.

[21] Wilcox, D.C., 1993 and 1998, Turbulence Modeling for CFD, DCW Industries, Inc.

[22] Kim, J., Kline, S.J., Johnston, J.P., 1980, Investigation of a reattaching turbulent shear layer: flow over backward-facing step. *ASME Journal of Fluids Engineering*, **102**, 302.

[23] Golub, G.H. and Van Loan, C.F., 1996, *Matrix Computations*, 3rd edition, (Baltimore, MD: John Hopkins University Press.

[24] Guo, Z.L., *et al.*, 2002, Non-equilibrium extrapolation method for velocity and pressure boundary conditions in the lattice Boltzmann method. *Chinese Physics*, **11**, 366.

[25] Succi, S., *et al.*, 1999, An integer lattice realization of a lax scheme for transport processes in multiple component fluid flows. *Journal of Computational Physics*, **152**, 493.

[26] Pervaiz, M.M. and Teixeira, C.M., 1999, Two equation turbulence modeling with the lattice Boltzmann method. *2nd Int. Symp. on Computational Technologies for Fluid/Thermal/Chemical Systems with Industrial Applications, ASME PVP Division Conf.*, 1–5 August 1999, Bosten, MA.

[27] Demirdzic, I.A., 1982, A finite volume method for computation of fluid flow in complex geometries *PhD Thesis* University of London.

[28] Nallasamy, N., 1987, Turbulence models and their applications to the prediction of internal flows: a review. *Computational Fluids*, **15**, 151.

[29] Thangam, S. and Speziale, C.G., 1991, Turbulent separated flow past a backward-facing step: a critical evaluation of two-equation turbulence models. ICASE Report 91-23.